







Mass bias and cosmological constraints from *Planck* cluster clustering

G. F. Lesci^{1,2}, A. Veropalumbo³, M. Sereno^{2,4}, F. Marulli^{1,2,4}, L. Moscardini^{1,2,4}, and C. Giocoli^{2,4}

¹ Dipartimento di Fisica e Astronomia “Augusto Righi” – Alma Mater Studiorum Università di Bologna, Via Piero Gobetti 93/2, 40129 Bologna, Italy

e-mail: giorgio.lesci2@unibo.it

² INAF – Osservatorio di Astrofisica e Scienza dello Spazio di Bologna, Via Piero Gobetti 93/3, 40129 Bologna, Italy

³ INAF – Osservatorio Astronomico di Brera, Via Brera 28, 20122 Milan, Via E. Bianchi 46, 20121 Merate, Italy

⁴ INFN – Sezione di Bologna, Viale Berti Pichat 6/2, 40127 Bologna, Italy

Received 27 February 2023 / Accepted 20 April 2023

ABSTRACT

Aims. We analysed the 3D clustering of the *Planck* sample of Sunyaev–Zeldovich (SZ) selected galaxy clusters, focusing on the redshift-space two-point correlation function (2PCF). We compared our measurements to theoretical predictions of the standard Λ cold dark matter (Λ CDM) cosmological model, deriving an estimate of the Planck mass bias, b_{SZ} , and cosmological parameters.

Methods. We measured the 2PCF of the sample in the cluster-centric radial range $r \in [10, 150] h^{-1}$ Mpc, considering 920 galaxy clusters with redshift $z \leq 0.8$. A Markov chain Monte Carlo analysis was performed to constrain b_{SZ} , assuming priors on cosmological parameters from *Planck* cosmic microwave background (CMB) results. We also adopted priors on b_{SZ} from external data sets to constrain the cosmological parameters Ω_m and σ_8 .

Results. We obtained $(1 - b_{SZ}) = 0.62^{+0.14}_{-0.11}$, which agrees with the value required to reconcile primary CMB and cluster count observations. By adopting priors on $(1 - b_{SZ})$ from external data sets, we derived results on Ω_m that fully agree and are competitive, in terms of uncertainties, with those derived from cluster counts. This confirms the importance of including clustering in cosmological studies in order to fully exploit the information from galaxy cluster statistics. On the other hand, we found that σ_8 is not constrained.

Key words. cosmological parameters – cosmology: observations – large-scale structure of Universe – galaxies: clusters: general

1. Introduction

Galaxy clusters are excellent tracers of the large-scale matter distribution of the Universe, probing its geometry and evolution through their abundance and clustering (Sereno et al. 2015; Veropalumbo et al. 2016; Costanzi et al. 2019; Marulli et al. 2021; Moresco et al. 2021; To et al. 2021; Lesci et al. 2022a; Euclid Collaboration 2022). In particular, the formation and evolution of galaxy clusters can theoretically be described with high accuracy through numerical simulations. This allows the theoretical calibration of the cluster halo mass and bias functions (Sheth & Tormen 1999; Sheth et al. 2001; Tinker et al. 2008, 2010; Despali et al. 2016; Euclid Collaboration 2023) and the description of the cluster dark matter profiles (Navarro et al. 1997; Baltz et al. 2009), providing the link between cluster local and statistical properties. In addition, cluster masses can be measured with high precision through weak gravitational lensing (Sereno et al. 2017; Bellagamba et al. 2019; Stern et al. 2019) and X-ray observations (Arnaud et al. 2010; Planck Collaboration XX 2014; Sereno & Ettori 2017). Moreover, cluster abundance and clustering are suitable probes for mass calibration if a cosmological model is assumed (Murata et al. 2019; Chiu et al. 2020; Lesci et al. 2022b).

As cosmological parameters are inferred with high precision in current cluster statistical analyses, accurate cluster mass calibrations are of critical importance. An incomplete assessment of systematic uncertainties affecting the derived masses may lead to significant biases in the cosmological constraints

(Planck Collaboration XXIV 2016; Abbott et al. 2020). Simulations show that X-ray masses are typically 10–15% underestimated due to the assumption of hydrostatic equilibrium, for which bulk motions and turbulence in the intra-cluster medium are neglected (Nagai et al. 2007; Meneghetti et al. 2010; Rasia et al. 2012; Le Brun et al. 2014). Weak-lensing mass estimates can also be biased by the inaccuracy of density profile models (Oguri & Hamana 2011), baryonic effects influencing the halo concentration (Henson et al. 2017; Shirasaki et al. 2018; Beltz-Mohrmann & Berlind 2021), halo orientation (Becker & Kravtsov 2011; Dietrich et al. 2014; Zhang et al. 2022), and projections (Simet et al. 2017; Melchior et al. 2017). As the biases in the weak-lensing mass estimates are theoretically better understood, weak-lensing observations are exploited for calibrating the main bias affecting X-ray masses, called hydrostatic bias, b_h (von der Linden et al. 2014; Hoekstra et al. 2015; Planck Collaboration XXIV 2016; Smith et al. 2016; Sereno & Ettori 2017). In particular, the relation between the X-ray mass, M_X , and the true mass, M_{tr} , is usually expressed as $M_X = (1 - b_h)M_{tr}$.

In this paper, we focus on the mass bias of the Sunyaev–Zeldovich (SZ) selected *Planck* clusters (Planck Collaboration XXIV 2016; Planck Collaboration XXVII 2016), which is referred to as the Planck mass bias, b_{SZ} . Planck cluster masses are expected to be biased low as they are derived from a scaling relation based on X-ray observations of 20 relaxed clusters at $z < 0.2$ (Arnaud et al. 2010; Planck Collaboration XX 2014). We obtained an estimate of b_{SZ} that is independent of

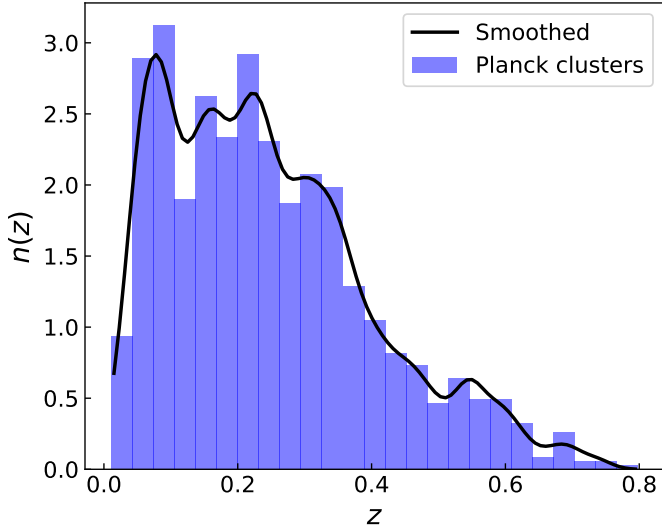


Fig. 1. Redshift distribution $n(z)$ of the galaxy clusters considered in the analysis. The blue histogram shows the observed binned $n(z)$, and the black curve represents $n(z)$ smoothed with a Gaussian kernel (with an rms equal to 0.02) that was used to build up the random catalogue.

lensing observations by exploiting the monopole of the 3D two-point correlation function (2PCF) of the galaxy clusters in the sample provided by [Planck Collaboration XXVII \(2016\)](#). In particular, we assumed a standard Λ cold dark matter (Λ CDM) cosmological model, adopting the cosmic microwave background (CMB) constraints on cosmological parameters from [Planck Collaboration VI \(2020\)](#) as priors. In addition, we adopted the same priors on $(1 - b_{SZ})$ as were used in the *Planck* cluster count analysis carried out by [Planck Collaboration XXIV \(2016\)](#) in order to constrain the matter density parameter, Ω_m , and the amplitude of the matter power spectrum, σ_8 .

The statistical analyses presented in this paper were performed with the CosmoBolognaLib¹ (CBL; [Marulli et al. 2016](#)), a set of free software C++/Python numerical libraries for cosmological calculations. Specifically, the measurements and the statistical Bayesian analyses were both performed with the CBL v6.1.

The paper is organised as follows. In Sect. 2 we describe the data set and the methods we used to estimate the 2PCF of the sample. In Sect. 3 we describe the 2PCF model, focusing on the dependence of the effective bias on the mass-observable scaling relation. In Sect. 4 we show our constraints on b_{SZ} and detail the cosmological analysis, and in Sect. 5 we draw our conclusions.

2. Data set and 2PCF measurement

2.1. The Planck cluster sample

Following [Planck Collaboration XXIV \(2016\)](#), we based our analysis on the cosmological sample consisting of detections by the MMF3 matched filter ([Melin et al. 2006, 2012](#)) derived from the general *Planck* full-mission Sunyaev–Zeldovich catalogue (PSZ2; [Planck Collaboration XXVII 2016](#)). We considered clusters with a confirmed counterpart in external data sets and an assigned redshift estimate (see Table 9 in [Planck Collaboration XXVII 2016](#)), with a redshift limit $z \leq 0.8$, for a total of 920 clusters. We applied this redshift cut to exclude

5 clusters that are isolated with respect to the bulk of the redshift distribution because they hindered the derivation of a reliable smoothed redshift distribution, which is necessary for the construction of the random sample (see Sect. 2.2). In addition, differently from [Planck Collaboration XXIV \(2016\)](#), we did not apply any cut in the signal-to-noise ratio (S/N). This does not imply any potential problems due to the reliability of the selection function at low S/N because our model does not rely on assumptions on the sample completeness (see Sect. 3.2).

2.2. Random catalogue

The random catalogue used for the 2PCF measurement is 100 times larger than the *Planck* cluster sample. We smoothed the observed redshift distribution, $n(z)$, with a Gaussian kernel with an rms equal to 0.02 (see Fig. 1). Then we extracted random redshifts from this distribution. Random RA–Dec pairs were extracted by following the sample angular selection function. It consists of the combination of the MMF3 survey mask², namely \mathcal{M}_s , the hole mask excluding contaminated regions (e.g., by stars or large galaxies), \mathcal{M}_h , and the error function completeness. Both \mathcal{M}_s and \mathcal{M}_h are equal to 0 if the region is masked, otherwise, they are equal to 1. The error function completeness is defined as ([Planck Collaboration XXIX 2014](#))

$$P(d|Y_{500}, \sigma_{Y_i}(\theta_{500}), q) = \frac{1}{2} \left[1 + \operatorname{erf} \left(\frac{Y_{500} - q\sigma_{Y_i}(\theta_{500})}{\sqrt{2}\sigma_{Y_i}(\theta_{500})} \right) \right], \quad (1)$$

where d is the Boolean detection state, $\operatorname{erf}(x)$ is the Gauss error function, and Y_{500} and θ_{500} are the observed SZ signal and the detection angular scale within a critical radius R_{500} , respectively. The latter is defined as the distance from the cluster centre inside which the mean density is 500 times the critical density of the Universe at the given redshift, z . M_{500} is defined as the mass enclosed within R_{500} . In Eq. (1), σ_{Y_i} is the standard deviation of pixels for a given patch i , computed by following [Melin et al. \(2006\)](#), and q is the S/N threshold. As we did not apply any S/N cut to the sample, q corresponds to the minimum threshold adopted by [Planck Collaboration XXVII \(2016\)](#) in the detection process, namely $q = 4.5$. In Eq. (1), we assumed the sample mean values of Y_{500} and θ_{500} . We verified that using the median values of these quantities does not introduce significant variations in the final results. Then we extracted random angular positions, for each of which we sampled a number in the range $[0, 1]$. When this number was higher than the product of \mathcal{M}_s , \mathcal{M}_h and $P(d|Y_{500}, \sigma_{Y_i}, q)$, the random angular position was rejected. As an alternative to the error function completeness in Eq. (1), we weighted the pairs in the 2PCF estimator (described in Sect. 2.3) by $1/\sigma_{Y_i}^{\text{norm}}$, where $\sigma_{Y_i}^{\text{norm}}$ is equal to σ_{Y_i} divided by its minimum value, namely $\sigma_{Y_i}^{\text{norm}} = \sigma_{Y_i}/\min(\sigma_{Y_i})$. We verified that this approach provides results that fully agreed with what was derived from the application of the error function completeness.

2.3. Clustering measurement

We estimated the redshift-space 2PCF monopole using the [Landy & Szalay \(1993, LS\)](#) estimator,

$$\xi(s) = \frac{N_{RR}}{N_{DD}} \frac{DD(s)}{RR(s)} - 2 \frac{N_{RR}}{N_{DR}} \frac{DR(s)}{RR(s)} + 1, \quad (2)$$

where $DD(s)$, $RR(s)$, and $DR(s)$ are the number of data–data, random–random, and data–random pairs with

² https://irsa.ipac.caltech.edu/data/Planck/release_2/ancillary-data/HFI_Products.html

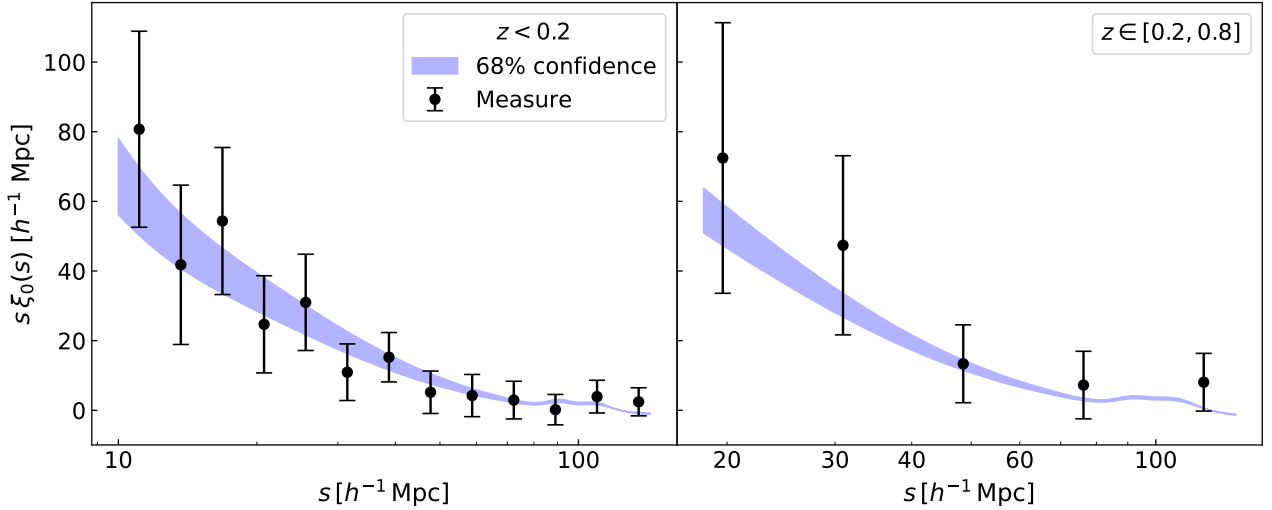


Fig. 2. Redshift-space 2PCF monopole (black dots) of the *Planck* clusters in the spatial range $s \in [10, 150] h^{-1} \text{ Mpc}$ for $z < 0.2$ (left plot), and $s \in [15, 150] h^{-1} \text{ Mpc}$ for $z \in [0.2, 0.8]$ (right plot). The blue bands represent the model 68% confidence level derived from the posterior of the free parameters considered in the analysis described in Sect. 4.1.

separation $s \pm \Delta s$, respectively, while N_{DD} , N_{RR} , and N_{DR} are the total number of data–data, random–random, and data–random pairs, respectively. To convert the observed coordinates into the comoving ones, we assumed the cosmological parameters by [Planck Collaboration VI \(2020\)](#), TT, TE, EE+lowE+lensing (referred to as [Planck18](#) hereafter). The LS estimator is extensively used in clustering analyses as it is unbiased with minimum variance for an infinitely large random sample and when $|\xi| \ll 1$ ([Hamilton 1992](#); [Kerscher et al. 2000](#); [Labatie et al. 2012](#); [Keihänen et al. 2019](#)).

Specifically, we measured the 2PCF considering two redshift bins, namely $z < 0.2$ and $z \in [0.2, 0.8]$, containing 407 and 513 galaxy clusters, respectively. We considered the cluster-centric radial range $s \in [10, 150] h^{-1} \text{ Mpc}$, excluding from the analysis the 2PCF measure at $s < 15 h^{-1} \text{ Mpc}$ in the second redshift bin due to the lack of data-data pairs. Moreover, we integrated the 2PCF measurements over larger s bins in $z \in [0.2, 0.8]$, compared to those adopted for the lower redshift bin. In this way, we compensated for the reduction of cluster pairs with small s distances, caused by the lower cluster density at high redshifts. We estimated the covariance matrix, including the cross-covariance between radial and redshift bins, through a bootstrap procedure. In particular, we considered 200 angular regions and two redshift regions, corresponding to the redshift bins, and resampled the observed and random catalogues 2000 times. We corrected the inverted covariance matrix following [Hartlap et al. \(2007\)](#). In Fig. 2 we show the measured 2PCF monopole, ξ_0 . We did not include the other non-zero multipoles in the analysis, as we verified that their contribution is negligible.

3. Modelling

We modelled the 2PCF of *Planck* clusters by accounting for geometric and redshift-space distortions. In addition, different to what was done in the *Planck* cluster count analysis by [Planck Collaboration XXIV \(2016\)](#), our model does not rely on assumptions on the sample completeness. We show in Sect. 4 that this approach leads to constraints on b_{SZ} and cosmological parameters that fully agree with those derived by [Planck Collaboration XXIV \(2016\)](#) and [Planck Collaboration VI \(2020\)](#).

3.1. Two-point correlation function model

The l th order 2PCF multipole, $\xi_l(s)$, can be expressed as follows:

$$\xi_l(s) = i^l \int_{-\infty}^{\infty} \frac{dk}{2\pi^2} k^2 P_l(k) j_l(ks), \quad (3)$$

where j_l is the spherical Bessel function of order l , and P_l is the redshift-space matter power spectrum multipole of order l ,

$$P_l(k) = \frac{2l+1}{2\alpha_{\perp}^2 \alpha_{\parallel}} \int_{-1}^1 d\mu P(k', \mu') L_l(\mu). \quad (4)$$

In Eq. (4), L_l is the Legendre polynomial of order l , and μ is the line of sight cosine. Moreover, in Eq. (4), we accounted for the [Alcock & Paczynski \(1979, AP\)](#) geometric distortions caused by the assumption of a fiducial cosmology used to convert the cluster observed coordinates into comoving ones in Eq. (2). Specifically, k' and μ' have the following functional forms ([Beutler et al. 2014](#)):

$$k' = \frac{k}{\alpha_{\perp}} \left[1 + \mu^2 \left(\frac{\alpha_{\perp}^2}{\alpha_{\parallel}^2} - 1 \right) \right]^{1/2}, \quad (5)$$

$$\mu' = \mu \frac{\alpha_{\perp}}{\alpha_{\parallel}} \left[1 + \mu^2 \left(\frac{\alpha_{\perp}^2}{\alpha_{\parallel}^2} - 1 \right) \right]^{-1/2}, \quad (6)$$

where α_{\perp} and α_{\parallel} are expressed as

$$\alpha_{\parallel} = \frac{H^{\text{fid}}(z) r_s^{\text{fid}}(z_d)}{H(z) r_s(z_d)}, \quad (7)$$

$$\alpha_{\perp} = \frac{D_A(z) r_s^{\text{fid}}(z_d)}{D_A^{\text{fid}}(z) r_s(z_d)}. \quad (8)$$

Here, $H^{\text{fid}}(z)$ and $D_A^{\text{fid}}(z)$ are the fiducial values for the Hubble constant and angular diameter distance, respectively, and $r_s^{\text{fid}}(z_d)$ is the fiducial sound horizon at the drag redshift, z_d . We stress that the AP correction takes place only in the cosmological analysis described in Sect. 4.3. To derive b_{SZ} , as detailed in Sect. 4.1,

we fixed the cosmological parameters to the fiducial ones. In Eq. (4), $P(k', \mu')$ is the redshift-space dark matter power spectrum expressed as (Taruya et al. 2010)

$$P(k', \mu') = D_{\text{FoG}}(k', \mu', f, \sigma_v) \left[b_{\text{eff}}^2 P_{\delta\delta}(k') + 2fb_{\text{eff}}\mu'^2 P_{\delta\theta}(k') + f^2\mu'^4 P_{\theta\theta}(k') + b_{\text{eff}}^3 A(k', \mu', f) + b_{\text{eff}}^4 B(k', \mu', f) \right], \quad (9)$$

where $P_{\delta\delta}$, $P_{\theta\theta}$, and $P_{\delta\theta}$ are the real-space auto power spectra of the density and velocity divergence and their cross power spectrum, respectively. These spectra are estimated in the standard perturbation theory (SPT), consisting of expanding the statistics as a sum of infinite terms, corresponding to the n -loop corrections (see e.g., Gil-Marín et al. 2012). Considering corrections up to the first-loop order, the power spectrum can be modelled as follows:

$$P^{\text{SPT}}(k) = P_{\text{L}}(k) + P^{(1)}(k) = P_{\text{L}}(k) + 2P_{13}(k) + P_{22}(k), \quad (10)$$

where the leading-order term, $P_{\text{L}}(k)$, is the linear matter power spectrum, computed with CAMB³ (Lewis & Challinor 2011), while the one-loop correction terms are computed with the CPT Library⁴ (Taruya & Hiramatsu 2008). In Eq. (9), $D_{\text{FoG}}(k', \mu', f, \sigma_v)$ is a Gaussian damping function representing the fingers-of-God effect, having the following functional form:

$$D_{\text{FoG}}(k', \mu', f, \sigma_v) = e^{-k'^2 \mu'^2 f^2 \sigma_v^2}, \quad (11)$$

where f is the linear growth rate, and σ_v^2 is the linear velocity dispersion, computed as (Taruya et al. 2010)

$$\sigma_v^2 = \frac{1}{3} \int \frac{d^3\mathbf{k}}{(2\pi)^3} \frac{P_{\text{L}}(k)}{k^2}. \quad (12)$$

In Eqs. (9) and (12), $P_{\text{L}}(k)$ is computed at the mean redshift of the cluster sub-sample in the given redshift bin. In addition, in Eq. (9), b_{eff} is the effective bias, defined in Sect. 3.2, and the functions $A(k', \mu', f)$ and $B(k', \mu', f)$ are correction terms derived from SPT (Taruya et al. 2010; de la Torre & Guzzo 2012; García-Farieta et al. 2020).

3.2. Effective bias

The effective bias, b_{eff} , has the following functional form:

$$b_{\text{eff}} = \frac{1}{N_{\text{cl}}} \sum_{j=1}^N b(Y_{500,j}^{\text{ob}}, z_j^{\text{ob}}), \quad (13)$$

where N_{cl} is the number of clusters in the sample, $Y_{500,j}^{\text{ob}}$ and z_j^{ob} are the observed SZ signal and redshift, respectively, of the j th cluster, and $b(Y_{500,j}^{\text{ob}}, z_j^{\text{ob}})$ is expressed as

$$b(Y_{500,j}^{\text{ob}}, z_j^{\text{ob}}) = \frac{1}{n(Y_{500,j}^{\text{ob}}, z_j^{\text{ob}})} \times \int_0^\infty dM_{500} \frac{dn(M_{500}, z_j^{\text{ob}})}{dM_{500}} b(M_{500}, z_j^{\text{ob}}) \times \int_0^\infty dY_{500} P(Y_{500}|M_{500}, z_j^{\text{ob}}) P(Y_{500}|Y_{500,j}^{\text{ob}}), \quad (14)$$

³ <https://camb.info/>

⁴ http://www2.yukawa.kyoto-u.ac.jp/~atsushi.taruya/cpt_pack.html

where $b(M_{500}, z)$ is the halo bias, for which the model by Tinker et al. (2010) was assumed, and $P(Y_{500}|Y_{500,j}^{\text{ob}})$ is a Gaussian whose mean is $Y_{500,j}^{\text{ob}}$ and its root mean square (rms) deviation is given by the error on $Y_{500,j}^{\text{ob}}$. In addition, $P(Y_{500}|M_{500}, z)$ is a log-normal whose mean is given by the mass-observable scaling relation, and its rms is given by the intrinsic scatter, $\sigma_{\ln Y}$,

$$P(\ln Y_{500}|M_{500}, z) = \frac{1}{\sqrt{2\pi}\sigma_{\ln Y}} e^{-\ln^2(Y_{500}/\bar{Y}_{500})/(2\sigma_{\ln Y}^2)}. \quad (15)$$

Specifically, following Planck Collaboration XXIV (2016), we assumed $\sigma_{\ln Y}$ to be independent of Y_{500} and redshift, and the expected value of SZ signal, \bar{Y}_{500} , can be expressed as

$$E^{-\beta}(z) \left[\frac{D_{\text{A}}^2(z) \bar{Y}_{500}}{10^{-4} \text{ Mpc}^2} \right] = Y_* \left[\frac{h}{0.7} \right]^{-2+\alpha} \left[\frac{(1 - b_{\text{SZ}}) M_{500}}{6 \times 10^{14} M_{\odot}} \right]^{\alpha}, \quad (16)$$

where $E(z) \equiv H(z)/H_0$, with $H(z)$ being the Hubble function and H_0 the Hubble constant, $D_{\text{A}}(z)$ is the angular diameter distance, $h \equiv H_0/100$, b_{SZ} is the Planck mass bias, and Y_* , α , and β are the scaling relation parameters. In addition, $n(Y_{500,j}^{\text{ob}}, z_j^{\text{ob}})$ in Eq. (14) is expressed as

$$n(Y_{500,j}^{\text{ob}}, z_j^{\text{ob}}) = \int_0^\infty dM_{500} \frac{dn(M_{500}, z_j^{\text{ob}})}{dM_{500}} \times \int_0^\infty dY_{500} P(Y_{500}|M_{500}, z_j^{\text{ob}}) P(Y_{500}|Y_{500,j}^{\text{ob}}), \quad (17)$$

where $dn(M_{500}, z)/dM_{500}$ is the halo mass function, for which the model by Tinker et al. (2008) was assumed.

3.3. Likelihood

For the Bayesian analysis performed in this work, a standard Gaussian likelihood was considered,

$$\mathcal{L} \propto \exp(-\chi^2/2), \quad (18)$$

with

$$\chi^2 = \sum_{i=1}^N \sum_{j=1}^N (\xi_i^d - \xi_i^m) C_{i,j}^{-1} (\xi_j^d - \xi_j^m), \quad (19)$$

where N is the number of comoving separation bins in which the 2PCF is computed, d and m indicate data and model, respectively, and $C_{i,j}^{-1}$ is the inverse of the covariance matrix. As detailed in Sect. 2.3, $C_{i,j}$ was derived through a bootstrap resampling.

4. Results

Based on the methods outlined in Sects. 2 and 3, we carried out an analysis of the redshift-space 2PCF monopole of the Planck cluster sample (Planck Collaboration XXVII 2016). Specifically, we detail in Sect. 4.1 the derivation of the $(1 - b_{\text{SZ}})$ constraint, performed by assuming the Planck18 cosmological results as priors. In Sect. 4.3 we present the constraints on cosmological parameters, obtained by assuming priors on b_{SZ} from external data sets.

Table 1. Free parameters considered in the analysis detailed in Sect. 4.1.

Parameter	Description	Prior	Posterior
b_{SZ}	Planck mass bias	$[-2, 0.9]$	$0.38^{+0.14}_{-0.11}$
$\log Y_*$	Normalisation of the mass-observable relation	$\mathcal{N}(-0.19, 0.02)$	–
α	Slope of the mass-observable relation	$\mathcal{N}(1.79, 0.08)$	–
β	Redshift evolution of the mass-observable relation	$\mathcal{N}(0.66, 0.50)$	–
$\sigma_{\ln Y}$	Intrinsic scatter of the mass-observable relation	$\mathcal{N}(0.173, 0.023)$	–

Notes. In the third column, the priors on the parameters are listed. In particular, a range between square brackets represents a uniform prior, and $\mathcal{N}(\mu, \sigma)$ stands for a Gaussian prior with mean μ and standard deviation σ . In the fourth column, we show the median values of the 1D marginalised posteriors, along with the 16th and 84th percentiles. The posterior distributions of $\log Y_*$, α , β , and $\sigma_{\ln Y}$ are not shown since these parameters are not constrained in our analysis.

4.1. Constraint on b_{SZ}

In order to derive a constraint on the Planck mass bias, b_{SZ} , we fixed the cosmological parameters to the [Planck18](#) median values. We also assumed the priors on the mass-observable scaling relation parameters in Eq. (16), namely Y_* , α , β , and $\sigma_{\ln Y}$, adopted by [Planck Collaboration XXIV \(2016\)](#). In particular, this scaling relation was derived from X-ray observations of 20 relaxed clusters at $z < 0.2$ ([Arnaud et al. 2010](#); [Planck Collaboration XX 2014](#)). Finally, we assumed a large flat prior on b_{SZ} . In Table 1 we summarise the priors used for this analysis, along with the result on the mass bias, namely $(1 - b_{SZ}) = 0.62^{+0.14}_{-0.11}$. The corresponding effective bias estimates are $b_{\text{eff}} = 4.61^{+0.39}_{-0.36}$ and $b_{\text{eff}} = 6.46^{+0.35}_{-0.37}$ for $z < 0.2$ and $z \in [0.2, 0.8]$, respectively. The constraint on $(1 - b_{SZ})$ is lower than what was predicted by numerical simulations ([Nagai et al. 2007](#); [Piffaretti & Valdarnini 2008](#); [Meneghetti et al. 2010](#); [Rasia et al. 2012](#); [Le Brun et al. 2017](#); [Henson et al. 2017](#); [Gianfagna et al. 2023](#)), but in line with what was found by [Planck Collaboration VI \(2020\)](#). We remark that even though the constraints on b_{eff} derived from the two redshift bins have similar associated uncertainties, our result on $(1 - b_{SZ})$ is dominated by the 2PCF signal measured at low redshift. We obtained $(1 - b_{SZ}) = 0.67^{+0.22}_{-0.13}$ for $z < 0.2$ and $(1 - b_{SZ}) = 0.58^{+0.55}_{-0.31}$ for $z \in [0.2, 0.8]$. This is expected because b_{eff} is directly derived from the mass-observable relation, and the number of clusters is comparable in the considered redshift bins. On the other hand, the constraints on $(1 - b_{SZ})$ depend on the 2PCF measurements, for which we obtained larger uncertainties in the high-redshift bin. In both redshift bins, we found $\chi^2_{\text{red}} \sim 0.9$, where χ^2_{red} is the reduced χ^2 . Specifically, we considered three effective free model parameters because the change in the model within the assumed priors on β and $\sigma_{\ln Y}$ is not statistically significant.

In Fig. 3 we show a comparison between our constraint on $(1 - b_{SZ})$ and the results obtained from the literature. In presence of systematic uncertainties, we added them in quadrature to the statistical ones. By combining primary CMB likelihood and cluster counts, [Planck Collaboration VI \(2020\)](#) derived $(1 - b_{SZ}) = 0.62 \pm 0.03$ (orange dot in Fig. 3), which fully agrees with our result. Regarding the Planck mass estimates derived from galaxy weak lensing, we found a 1σ agreement with Weighting the Giants (WtG; [von der Linden et al. 2014](#)), the Canadian Cluster Comparison Project (CCCP; [Hoekstra et al. 2015](#)), the Literature Catalogs of weak Lensing Clusters of galaxies (LC²; [Sereno & Ettori 2017](#)), the Cluster Lensing And Supernova survey with *Hubble* (CLASH; [Penna-Lima et al. 2017](#)), and the Subaru Hyper Suprime-Cam (HSC; [Medezinski et al. 2018](#)). We found an agreement of only 2σ with the results from the Local Cluster Substructure Survey

(LoCuSS; [Smith et al. 2016](#)), the Multi Epoch Nearby Cluster Survey (MENeCS) combined with updated mass weak-lensing estimates in CCCP (MENeCS+CCCP; [Herbonnet et al. 2020](#)), and with the result obtained from CMB lensing by [Planck Collaboration XXIV \(2016\)](#), however. When comparing our results to other analyses based on cluster counts, we found an agreement of 1σ with [Zubeldia & Challinor \(2019\)](#), and [Salvati et al. \(2019, 2022\)](#). Concerning the results derived from the power spectra of the *Planck* thermal Sunyaev–Zeldovich effect, our constraint agrees within 1σ with [Makiya et al. \(2018\)](#) and [Ibitoye et al. \(2022\)](#). We also found a good agreement with the constraint by [Wicker et al. \(2022\)](#) based on measurements of the cluster gas mass fraction. The hydrostatic bias estimates from dynamical masses by [Ferragamo et al. \(2021\)](#) and [Aguado-Barahona et al. \(2022\)](#) agree with our result within 1σ . In Sect. 4.2 we discuss the impact of the adopted modelling choices on our result, finding that the derived constraint on b_{SZ} is robust with respect to the investigated systematic uncertainties.

As many observational studies claimed a redshift dependence of the hydrostatic bias ([Smith et al. 2016](#); [Sereno & Ettori 2017](#); [Salvati et al. 2019, 2022](#); [Wicker et al. 2022](#)), we investigated this possibility by expressing b_{SZ} as follows:

$$b_{SZ} = \eta \left(\frac{1+z}{1+z_{\text{piv}}} \right)^{\zeta}, \quad (20)$$

where $z_{\text{piv}} = 0.25$ is the mean redshift of the sample, η is the normalisation, and ζ parametrises the redshift dependence of the mass bias. Our analysis does not constrain ζ , implying that it is not necessary to explain our data. We stress that the redshift dependence of b_{SZ} was derived from cluster statistics only in the case of a strong prior on the total value of b_{SZ} , with a significant dependence on the sample ([Salvati et al. 2019, 2022](#); [Wicker et al. 2022](#)).

4.2. Assessment of systematics on b_{SZ}

To assess the robustness of the constraint on b_{SZ} derived in Sect. 4.1, we included the power spectrum damping due to redshift uncertainties in the analysis. No redshift errors are quoted in *Planck* data products, and therefore, we expressed this damping by means of a free parameter. Specifically, we replaced Eq. (12) by the following expression:

$$\sigma_{v,\text{tot}} = \sqrt{\sigma_v^2 + \sigma_{v,z}^2}, \quad (21)$$

where σ_v is defined in Eq. (12), while $\sigma_{v,z}$ is the velocity dispersion caused by redshift errors, having the following functional

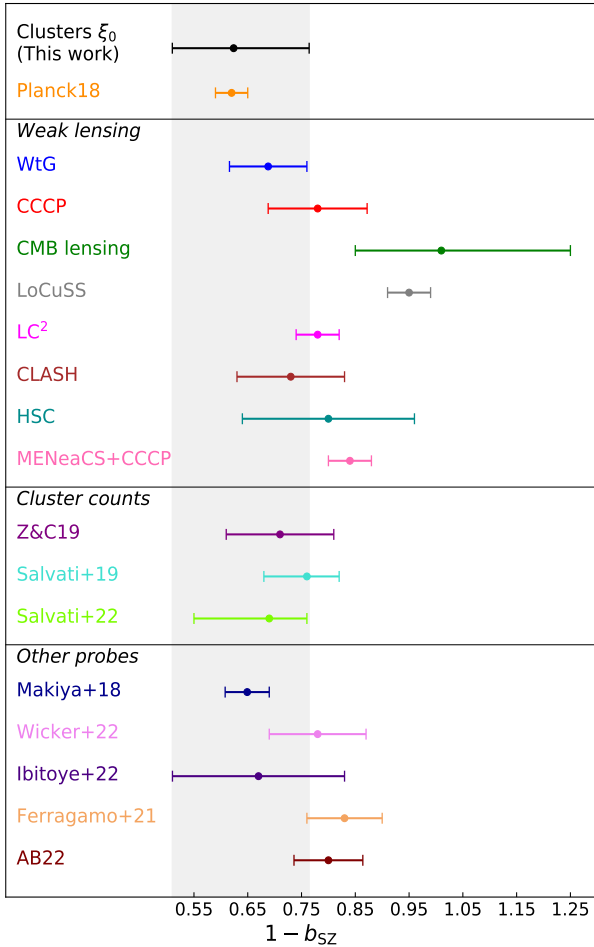


Fig. 3. Comparison of the results on $(1 - b_{SZ})$ with the literature. The median, 16th and 84th percentiles are shown. The black dot shows the constraint derived in this work. Then, in order from top to bottom, the following results are shown: [Planck Collaboration VI \(2020; orange\)](#), [von der Linden et al. \(2014; blue\)](#) [Hoekstra et al. \(2015; red\)](#), [Planck Collaboration XXIV \(2016; dark green\)](#), [Smith et al. \(2016; grey\)](#), [Sereno & Ettori \(2017; magenta\)](#), [Penna-Lima et al. \(2017; brown\)](#), [Medezinski et al. \(2018; cyan\)](#), [Herbonnet et al. \(2020; pink\)](#), [Zubeldia & Challinor \(2019; purple\)](#), [Salvati et al. \(2019; turquoise\)](#), [Salvati et al. \(2022; green\)](#), [Makiya et al. \(2018; dark blue\)](#), [Wicker et al. \(2022; violet\)](#), [Ibitoye et al. \(2022; indigo\)](#), [Ferragamo et al. \(2021; orange\)](#), and [Aguado-Barahona et al. \(2022; dark brown\)](#).

form:

$$\sigma_{v,z} \equiv \frac{c \sigma_z (1 + \bar{z})}{H(\bar{z})}. \quad (22)$$

In this equation, \bar{z} is the mean redshift of the sub-sample in a given redshift bin, c is the speed of light, $H(z)$ is the Hubble function, and σ_z is the typical redshift uncertainty of the sample. By assuming a flat prior on σ_z , namely $\sigma_z \in [0, 0.1]$, we derived $\sigma_z = 0.003^{+0.002}_{-0.002}$, which is in line with the fact that most of the cluster redshifts are spectroscopic, and $(1 - b_{SZ}) = 0.65^{+0.15}_{-0.12}$, which fully agrees with our previous result.

In addition, we analysed the 2PCF monopole of the *Planck* union catalogue, containing the clusters detected with the three detection algorithms adopted by [Planck Collaboration XXVII \(2016\)](#). By assuming the same sample selections and bins of redshift and radius described in Sect. 2, we found $(1 - b_{SZ}) = 0.59^{+0.12}_{-0.09}$, which is in line with the constraint derived in Sect. 4.1.

This implies that our result is independent of the adopted cluster detection algorithm. We also performed the analysis by considering the clusters in the MMF3 sample with $S/N > 6$, and for which the COSMO entry in the union catalogue is set to ‘T’, meaning that these clusters are part of the cosmological sample, following [Planck Collaboration XXIV \(2016\)](#). Because the statistics are poorer in this case, we analysed the 2PCF in a single redshift bin including clusters with $z \leq 0.8$ for a total of 430 objects. As the modelling provides reduced χ^2 estimates that are not close to 1, we conclude that in this case, the 2PCF signal does not allow a reliable constraint on b_{SZ} .

In order to further assess the robustness of our results on $(1 - b_{SZ})$, we computed the 2PCF model at the sample median redshifts for each redshift bin, instead of adopting the mean redshift, as discussed in Sect. 3. In this way, we derived a shift of the median $(1 - b_{SZ})$ of $\sim 0.006\sigma$. In addition, the reduction of the 2PCF radial range to $s \in [15, 150] h^{-1}$ Mpc or to $s \in [10, 90] h^{-1}$ Mpc implies comparable results, namely shifts of the median $(1 - b_{SZ})$ lower than $\sim 0.6\sigma$, and variations in the 1σ interval extension lower than $\sim 50\%$. We also checked the impact of a change in the definition of the effective bias, b_{eff} , assuming the median of the halo bias distribution instead of considering its mean, as done in Eq. (13). In this case, we obtained a shift of the median $(1 - b_{SZ})$ corresponding to $\sim 0.5\sigma$. As the tests described above showed shifts in the median b_{SZ} that are within 1σ of the constraint presented in Sect. 4.1, we can conclude that our results are robust with respect to the investigated modelling choices. Lastly, [Salvati et al. \(2020\)](#) showed that the impact of the halo mass function calibration has a subdominant impact on current cluster count analyses. It will become a relevant source of systematic errors in upcoming surveys, for instance those from *Euclid* ([Laureijs et al. 2011](#)) and the Large Synoptic Survey Telescope ([LSST Science Collaboration 2009](#)), because of the larger cluster statistics they will provide. As cluster clustering has a lower constraining power compared to counts, we expect the mass function calibration to provide a negligible impact on the b_{SZ} constraints derived in this work. The same is expected for the halo bias calibration.

4.3. Constraints on cosmological parameters

To further investigate the consistency of our modelling choices with those adopted by [Planck Collaboration XXIV \(2016\)](#), we performed a cosmological analysis aiming at constraining σ_8 and Ω_m simultaneously by assuming the same Gaussian priors on b_{SZ} as were considered by [Planck Collaboration XXIV \(2016\)](#). Specifically, we assumed large flat priors for σ_8 and Ω_m , while for the other cosmological parameters, we assumed the same values from [Planck18](#) that were used in the previous section. We also assumed the same Gaussian priors as adopted in Sect. 4.1 on the scaling relation parameters, namely Y_s , α , β , and $\sigma_{\ln Y}$. We found that σ_8 is not constrained through this analysis, while we found $\Omega_m = 0.28^{+0.05}_{-0.04}$ with the WtG b_{SZ} prior, $\Omega_m = 0.28^{+0.04}_{-0.03}$ with the CCCP prior, and $\Omega_m = 0.27^{+0.04}_{-0.03}$ with the CMB lensing prior (see Fig. 4). These results are fully consistent and competitive, in terms of uncertainties, with those derived by [Planck Collaboration XXIV \(2016\)](#). Similar uncertainties on Ω_m were obtained by [Marulli et al. \(2018\)](#) and [Lindholm et al. \(2021\)](#), who modelled the 2PCF of 182 and 1892 X-ray selected galaxy clusters, respectively. In addition, [Marulli et al. \(2018\)](#) found that σ_8 could not be accurately constrained, in agreement with our results. In general, recent analyses of cluster clustering showed that the constraints on Ω_m are significantly more robust than those derived on σ_8 ([Lindholm et al. 2021](#); [Lesci et al. 2022b](#)).

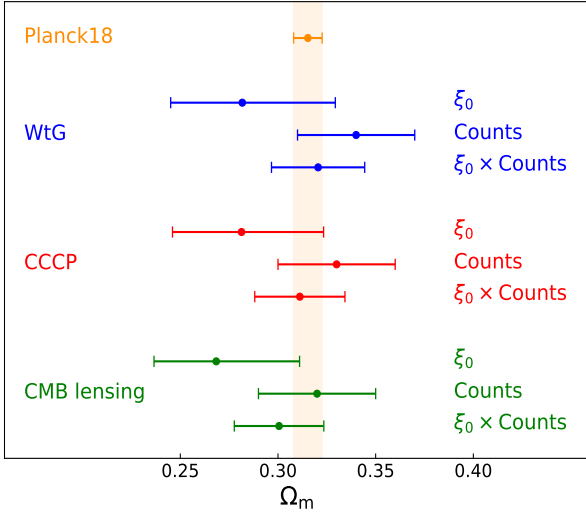


Fig. 4. Comparison of the results on Ω_m obtained by assuming flat priors on Ω_m and σ_8 , along with external priors on b_{SZ} , namely WtG (blue; von der Linden et al. 2014), CCCP (red; Hoekstra et al. 2015) and CMB lensing (green; Planck Collaboration XXIV 2016). For each b_{SZ} prior, the result at the top was derived from the cluster clustering measurements presented in this paper, the middle result refers to the cluster counts analysis by Planck Collaboration XXIV (2016), and the bottom result represents the combination of *Planck* cluster clustering and counts. The constraint from Planck18 is shown in orange.

In addition, we note that significant changes in the value of b_{SZ} do not imply significant variations in the Ω_m posteriors, similar to what was found by Planck Collaboration XXIV (2016).

We also derived an estimate of Ω_m from the combination of cluster clustering and counts by assuming them to be statistically independent. Hurier & Lacasa (2017) showed that cluster counts and thermal SZ power spectrum are not significantly correlated. The thermal SZ power spectrum mainly depends on massive haloes, while for the number counts, the main contribution comes from lower-mass halos. The differences between the two galaxy cluster populations imply a weak correlation of these probes. As the clustering of SZ selected clusters encloses the same information contained in the SZ power spectrum, we expect a similar behavior for its correlation with counts. With respect to the analysis based on counts only, we found that the uncertainty on Ω_m is reduced by a factor of $\sim 25\%–30\%$ if clustering is included in the likelihood. This confirms the importance of including cluster clustering in cosmological analyses (see also Sartoris et al. 2016; Euclid Collaboration 2022; Garrel et al. 2022) in order to fully exploit the cluster statistics information.

5. Summary and discussion

We analysed the 3D 2PCF monopole of the galaxy clusters detected by Planck Collaboration XXVII (2016), focusing on the estimate of the Planck mass bias, b_{SZ} . Following Planck Collaboration XXIV (2016), we based our analysis on the cosmological sample consisting of detections by the MMF3 matched filter (Melin et al. 2006, 2012), considering clusters with a confirmed counterpart in external data sets and having an assigned redshift estimate, with a redshift limit $z \leq 0.8$, for a total of 920 clusters. Differently from Planck Collaboration XXIV (2016), we did not apply any cut in S/N to the sample. This does not imply any potential prob-

lems due to the reliability of the selection function at low S/N because our model does not rely on assumptions on the sample completeness.

By analysing the 2PCF in the redshift bins $z < 0.2$ and $z \in [0.2, 0.8]$ within the cluster-centric radial range $r \in [10, 150] h^{-1}$ Mpc, we derived $(1 - b_{SZ}) = 0.62^{+0.14}_{-0.11}$. This result fully agrees with what was found by Planck Collaboration VI (2020) by combining primary CMB likelihood and *Planck* cluster counts. Thus, we confirmed that *Planck* cluster statistics provides values of b_{SZ} that are lower than what was predicted by numerical simulations (Nagai et al. 2007; Piffaretti & Valdarnani 2008; Meneghetti et al. 2010; Rasia et al. 2012; Le Brun et al. 2017; Henson et al. 2017; Gianfagna et al. 2023). As redshift errors are not quoted in *Planck* data products, we also included the power spectrum damping due to redshift uncertainties by means of a free parameter representing the typical redshift error, namely σ_z . Thus, we simultaneously calibrated σ_z and b_{SZ} , finding no significant changes in b_{SZ} and $\sigma_z = 0.003^{+0.002}_{-0.002}$, which is in line with the fact that most of the cluster redshifts are spectroscopic. In addition, from the analysis of the *Planck* union catalogue of clusters, we showed that our result does not depend on the adopted cluster detection algorithm. We also found that a redshift evolution of b_{SZ} is not necessary to describe our clustering measurements.

By adopting priors on b_{SZ} from external data sets, we found results on Ω_m that fully agree and are competitive, in terms of uncertainties, with those derived from cluster counts by Planck Collaboration XXIV (2016), while σ_8 is not constrained. By assuming cluster clustering and counts to be statistically independent, we found that their combination provides a reduction of up to $\sim 30\%$ in the Ω_m uncertainty derived from counts. Future stage-4 CMB experiments (Abazajian et al. 2016) will detect about 10^5 galaxy clusters through the SZ effect, which will significantly enhance the cluster statistical analyses. This will improve the calibration of the hydrostatic mass bias from cluster clustering, and might shed light on the degeneracy between σ_8 and mass bias. This degeneracy cannot be investigated with current data because σ_8 is not constrained, as we detailed in Sect. 4.3. As a consequence, along with cluster abundance, cluster clustering will play a crucial role in the understanding of the current cosmological tensions between early and late Universe observations.

Acknowledgements. We acknowledge support from the grants PRIN-MIUR 2017 WSCC32 and ASI n.2018-23-HH.0. GC thanks the support from INAF theory Grant 2022: Illuminating Dark Matter using Weak Lensing by Cluster Satellites, PI: Carlo Giocoli. MS acknowledges financial contributions from contract ASI-INAF n.2017-14-H.0 and contract INAF mainstream project 1.05.01.86.10.

References

- Abazajian, K. N., Adshead, P., Ahmed, Z., et al. 2016, ArXiv e-prints [arXiv:1610.02743]
- Abbott, T. M. C., Aguena, M., Alarcon, A., et al. 2020, *Phys. Rev. D*, **102**, 023509P
- Aguado-Barahona, A., Rubiño-Martín, J. A., Ferragamo, A., et al. 2022, *A&A*, **659**, A126
- Alcock, C., & Paczynski, B. 1979, *Nature*, **281**, 358
- Arnaud, M., Pratt, G. W., Piffaretti, R., et al. 2010, *A&A*, **517**, A92
- Baltz, E. A., Marshall, P., & Oguri, M. 2009, *J. Cosmol. Astropart. Phys.*, **1**, 15
- Becker, M. R., & Kravtsov, A. V. 2011, *ApJ*, **740**, 25
- Bellagamba, F., Sereno, M., Roncarelli, M., et al. 2019, *MNRAS*, **484**, 1598
- Beltz-Mohrmann, G. D., & Berlind, A. A. 2021, *ApJ*, **921**, 112
- Beutler, F., Saito, S., Seo, H.-J., et al. 2014, *MNRAS*, **443**, 1065
- Chiu, I. N., Okumura, T., Oguri, M., et al. 2020, *MNRAS*, **498**, 2030
- Costanzi, M., Rozo, E., Simet, M., et al. 2019, *MNRAS*, **488**, 4779
- de la Torre, S., & Guzzo, L. 2012, *MNRAS*, **427**, 327

- Despali, G., Giocoli, C., Angulo, R. E., et al. 2016, *MNRAS*, **456**, 2486
- Dietrich, J. P., Zhang, Y., Song, J., et al. 2014, *MNRAS*, **443**, 1713
- Euclid Collaboration (Fumagalli, A., et al.) 2022, ArXiv e-prints [arXiv:2211.12965]
- Euclid Collaboration (Castro, T., et al.) 2023, *A&A*, **671**, A100
- Ferragamo, A., Barrena, R., Rubiño-Martín, J. A., et al. 2021, *A&A*, **655**, A115
- García-Farieta, J. E., Marulli, F., Moscardini, L., Veropalumbo, A., & Casas-Miranda, R. A. 2020, *MNRAS*, **494**, 1658
- Garrel, C., Pierre, M., Valageas, P., et al. 2022, *A&A*, **663**, A3
- Gianfagna, G., Rasia, E., Cui, W., et al. 2023, *MNRAS*, **518**, 4238
- Gil-Marín, H., Wagner, C., Verde, L., Porciani, C., & Jimenez, R. 2012, *J. Cosmol. Astropart. Phys.*, **11**, 29
- Hamilton, A. J. S. 1992, *ApJ*, **385**, L5
- Hartlap, J., Simon, P., & Schneider, P. 2007, *A&A*, **464**, 399
- Henson, M. A., Barnes, D. J., Kay, S. T., McCarthy, I. G., & Schaye, J. 2017, *MNRAS*, **465**, 3361
- Herbonnet, R., Sifón, C., Hoekstra, H., et al. 2020, *MNRAS*, **497**, 4684
- Hoekstra, H., Herbonnet, R., Muzzin, A., et al. 2015, *MNRAS*, **449**, 685
- Hurier, G., & Lacasa, F. 2017, *A&A*, **604**, A71
- Ibitoye, A., Tramonte, D., Ma, Y.-Z., & Dai, W.-M. 2022, *ApJ*, **935**, 18
- Keihänen, E., Kurki-Suonio, H., Lindholm, V., et al. 2019, *A&A*, **631**, A73
- Kerscher, M., Szapudi, I., & Szalay, A. S. 2000, *ApJ*, **535**, L13
- Labatie, A., Starck, J. L., Lachièze-Rey, M., & Arnalte-Mur, P. 2012, *Stat. Methodol.*, **9**, 85
- Landy, S. D., & Szalay, A. S. 1993, *ApJ*, **412**, 64
- Laureijs, R., Amiaux, J., Arduini, S., et al. 2011, ArXiv e-prints [arXiv:1110.3193]
- Le Brun, A. M. C., McCarthy, I. G., Schaye, J., & Ponman, T. J. 2014, *MNRAS*, **441**, 1270
- Le Brun, A. M. C., McCarthy, I. G., Schaye, J., & Ponman, T. J. 2017, *MNRAS*, **466**, 4442
- Lesci, G. F., Marulli, F., Moscardini, L., et al. 2022a, *A&A*, **659**, A88
- Lesci, G. F., Nanni, L., Marulli, F., et al. 2022b, *A&A*, **665**, A100
- Lewis, A., & Challinor, A. 2011, Astrophysics Source Code Library [record ascl:1102.026]
- Lindholm, V., Finoguenov, A., Comparat, J., et al. 2021, *A&A*, **646**, A8
- LSST Science Collaboration (Abell, P. A., et al.) 2009, ArXiv e-prints [arXiv:0912.0201]
- Makiya, R., Ando, S., & Komatsu, E. 2018, *MNRAS*, **480**, 3928
- Marulli, F., Veropalumbo, A., & Moresco, M. 2016, *Astron. Comput.*, **14**, 35
- Marulli, F., Veropalumbo, A., Sereno, M., et al. 2018, *A&A*, **620**, A1
- Marulli, F., Veropalumbo, A., García-Farieta, J. E., et al. 2021, *ApJ*, **920**, 13
- Medezinski, E., Battaglia, N., Umetsu, K., et al. 2018, *PASJ*, **70**, S28
- Melchior, P., Gruen, D., McClintock, T., et al. 2017, *MNRAS*, **469**, 4899
- Melin, J. B., Bartlett, J. G., & Delabrouille, J. 2006, *A&A*, **459**, 341
- Melin, J. B., Aghanim, N., Bartelmann, M., et al. 2012, *A&A*, **548**, A51
- Meneghetti, M., Rasia, E., Merten, J., et al. 2010, *A&A*, **514**, A93
- Moresco, M., Veropalumbo, A., Marulli, F., Moscardini, L., & Cimatti, A. 2021, *ApJ*, **919**, 144
- Murata, R., Oguri, M., Nishimichi, T., et al. 2019, *PASJ*, **71**, 107
- Nagai, D., Vikhlinin, A., & Kravtsov, A. V. 2007, *ApJ*, **655**, 98
- Navarro, J. F., Frenk, C. S., & White, S. D. M. 1997, *ApJ*, **490**, 493
- Oguri, M., & Hamana, T. 2011, *MNRAS*, **414**, 1851
- Penna-Lima, M., Bartlett, J. G., Rozo, E., et al. 2017, *A&A*, **604**, A89
- Piffaretti, R., & Valdarnini, R. 2008, *A&A*, **491**, 71
- Planck Collaboration XX. 2014, *A&A*, **571**, A20
- Planck Collaboration XXIX. 2014, *A&A*, **571**, A29
- Planck Collaboration XXIV. 2016, *A&A*, **594**, A24
- Planck Collaboration XXVII. 2016, *A&A*, **594**, A27
- Planck Collaboration VI. 2020, *A&A*, **641**, A6
- Rasia, E., Meneghetti, M., Martino, R., et al. 2012, *New J. Phys.*, **14**, 055018
- Salvati, L., Douspis, M., Ritz, A., Aghanim, N., & Babul, A. 2019, *A&A*, **626**, A27
- Salvati, L., Douspis, M., & Aghanim, N. 2020, *A&A*, **643**, A20
- Salvati, L., Saro, A., Bocquet, S., et al. 2022, *ApJ*, **934**, 129
- Sartoris, B., Biviano, A., Fedeli, C., et al. 2016, *MNRAS*, **459**, 1764
- Sereno, M., & Ettori, S. 2017, *MNRAS*, **468**, 3322
- Sereno, M., Veropalumbo, A., Marulli, F., et al. 2015, *MNRAS*, **449**, 4147
- Sereno, M., Covone, G., Izzo, L., et al. 2017, *MNRAS*, **472**, 1946
- Sheth, R. K., & Tormen, G. 1999, *MNRAS*, **308**, 119
- Sheth, R. K., Mo, H. J., & Tormen, G. 2001, *MNRAS*, **323**, 1
- Shirasaki, M., Lau, E. T., & Nagai, D. 2018, *MNRAS*, **477**, 2804
- Simet, M., McClintock, T., Mandelbaum, R., et al. 2017, *MNRAS*, **466**, 3103
- Smith, G. P., Mazzotta, P., Okabe, N., et al. 2016, *MNRAS*, **456**, L74
- Stern, C., Dietrich, J. P., Bocquet, S., et al. 2019, *MNRAS*, **485**, 69
- Taruya, A., & Hiramatsu, T. 2008, *ApJ*, **674**, 617
- Taruya, A., Nishimichi, T., & Saito, S. 2010, *Phys. Rev. D*, **82**, 063522
- Tinker, J., Kravtsov, A. V., Klypin, A., et al. 2008, *ApJ*, **688**, 709
- Tinker, J. L., Robertson, B. E., Kravtsov, A. V., et al. 2010, *ApJ*, **724**, 878
- To, C., Krause, E., Rozo, E., et al. 2021, *Phys. Rev. Lett.*, **126**, 141301
- Veropalumbo, A., Marulli, F., Moscardini, L., Moresco, M., & Cimatti, A. 2016, *MNRAS*, **458**, 1909
- von der Linden, A., Mantz, A., Allen, S. W., et al. 2014, *MNRAS*, **443**, 1973
- Wicker, R., Douspis, M., Salvati, L., & Aghanim, N. 2022, *Eur. Phys. J. Web Conf.*, **257**, 00046
- Zhang, Z., Wu, H. Y., Zhang, Y., et al. 2022, ArXiv e-prints [arXiv:2202.08211]
- Zubeldia, Í., & Challinor, A. 2019, *MNRAS*, **489**, 401